

Design and Synthesis of Ternary Graphene/Polyaniline/Co₃O₄ Hierarchical Nanocomposites for Supercapacitors

Hongzhi Wang, Zhenyu Guo, Suwei Yao, Zixuan Li, Weiguo Zhang*

Department of Applied Chemistry, School of Chemical Engineering and Technology, Tianjin University, Tianjin 300350, P. R. China

*E-mail: zwg@tju.edu.cn

Received: 13 February 2017 / Accepted: 9 March 2017 / Published: 12 April 2017

Graphene/polyaniline/Co₃O₄ ternary composites were synthesized by a facile route using graphene oxide/polyaniline (GO/PANI) and cobalt salts as raw materials through hydrothermal treatment. The composites prepared by the novel two-step method presented an interconnected lamella structure in which the Co₃O₄ nanoparticles uniformly dispersed on the ultrathin graphene nanosheets, and exhibited an outstanding performance with large specific capacitance of 789.7 F g⁻¹ at a current density of 1 A g⁻¹. Furthermore, their capacitance retained 81.8% at 10 A g⁻¹ for 1000 cycles, which indicated it could be a promising supercapacitor with a superior capacitance and cycling stability.

Keywords: Supercapacitors, Graphene, PANI, Co₃O₄, Two-step method

1. INTRODUCTION

Supercapacitors are reliable energy storage devices which have evoked numerous research attentions owing to their outstanding reversibility, high power density and long cycle life [1-3]. Based on their charge-storage mechanisms, supercapacitors could be categorized as pseudocapacitors or electrochemical double layer capacitors (EDLCs) [4]. EDLCs, generally utilizing carbon materials as the electrode often have a high power density because of the nondegradative process [5-7]. Among carbon materials, graphene is a potential candidate as an electrode material for EDLCs due to its superior conductivity, large specific surface area and environmental friendliness [7, 8]. However, the practical applications of graphene based electrode materials are still seriously hindered due to the unsatisfactory performance such as the low specific capacitance because of its easy agglomeration [9]. Therefore, graphene composites with transition metal oxides or conductive polymers which can deliver a higher capacitance have been considered as the electrode materials with great promise [10,

11]. Thus, many materials with conductive polymers attached to graphene were synthesized, which could not only obviously increase the specific capacitance, but also avoid the aggregation of graphene sheets.

As one of the most promising materials among conducting polymers, polyaniline (PANI) has attracted extensive interest for its excellent specific capacitance (2000 F/g), high conductivity, low-cost, easy synthesis, stable chemical properties [12-14]. Metal ions can be effectively linked with the N atoms in polyaniline to reconcile their hydrothermal process to fabricate polyaniline/metal oxide nanoparticles [15]. Recently, many ternary graphene/polyaniline/transition metal oxide were reported as supercapacitors such as MnO_2 [16, 17], TiO_2 [18], and Co_3O_4 [19]. But it's intricate to synthesize all of these materials, which is still subjected to the problem of electrochemical stability.

Transition metal oxides have been researched for their promising application as electrodes in energy storage devices. Among transition metal oxides, Co_3O_4 has attracted interest owing to its large specific capacitance (3560 F/g), relatively low cost and superior stability [20, 21]. The critical problem that hinders the application of Co_3O_4 in energy storage is its poor power density by the slow faradic reaction and electron transport. So it is an effective method to promote the faradic reaction and electron transport by interconnecting graphene materials with Co_3O_4 .

In this work, we presented a simple method to synthesize a novel lamella structure of ternary graphene/polyaniline/ Co_3O_4 (GPC) hybrid as a promising supercapacitor material. The pre-nanocomposite graphene oxide/polyaniline (GO/PANI) was prepared by a facile in situ polymerization of aniline in the presence of GO. The subsequent preparation involves a self-assembly of cobalt salts in the presence of GO/PANI to form RGO/PANI/ Co_3O_4 through hydrothermal treatment. An excellent specific capacitance and a long cycling life could be reached because the ternary composite is supposed to avoid the defects of each component. As a result, extraordinary performance was achieved with high specific capacitance of 789.7 F/g at a current density of 1 A/g. And a capacitance retention of 81.8 % at 10 A/g was observed after 1000 cycles, making the composite a potential long-lived electrode material for energy storage devices.

2. EXPERIMENTAL

2.1. Synthesis of RGO/PANI/ Co_3O_4

Firstly graphite oxide (GO) nanosheets were prepared by the modified Hummers method [22]. 30mg GO was added to 50 mL 1 M HCl solution at ultrasonic for 90 min to form a uniform suspension. Subsequently, 80 μL aniline was dispersed in the above solution. Then, 0.25g APS in 10 mL 1 M HCl was dropped into the suspension slowly which was stirred for 3 h at room temperature. The resulting mixture was centrifuged with DI water to obtain the graphene oxide/polyaniline (GO/PANI) hybrid. Secondly, $\text{CoCl}_2 \cdot 6\text{H}_2\text{O}$ (237.93 mg, 1mmol) was dissolved in 50 mL DI water, then the above solution was added into 25 mL GO/PANI hybrid suspension followed by stirring for 2 h at room temperature. The resulting mixture was transferred to a 70 mL vial, which was then removed into a 100 mL Teflon-lined stainless steel autoclave for hydrothermal treatment at 160 °C for 6 h to

obtain RGO/PANI/Co₃O₄ after drying in a vacuum oven for 12 hours. For comparison, RGO/PANI was synthesized with the similar method above without CoCl₂·6H₂O. The reduced graphene oxide (RGO) could be obtained after hydrothermal process of graphene oxide (GO).

2.2. Characterization

The morphologies of the samples were observed by scanning electron microscopy (SEM, S-4800, HITACHI, Japan) and the detailed microscopic structure was characterized by transmission electron microscopy (TEM, JEM-2100, JEOL, Japan). The crystalline phase was established with an X-ray diffraction (XRD, 40 kV, 200 mA, Rigaku, Mutiflex, D/MAX-2500, Japan) using Cu-K α radiation ($\lambda = 1.5406 \text{ \AA}$) over the 2θ range from 10 to 70°. Thermogravimetric analysis (TGA) was performed on a TG8120 by heating the sample at the rate of 10°C min⁻¹ in the atmosphere of air. A DXR Raman Microscope was applied to record Raman Spectra using a 532 nm laser beam. The X-ray photoelectron spectra (XPS) was carried out on a PHI-1600 photoelectron spectrometer with Al K α radiation ($h\nu = 1486.6 \text{ eV}$).

2.3. Electrochemical measurements

Cyclic voltammetry (CV), galvanostatic charge/discharge test, and electrochemical impedance spectroscopy (EIS) measurements were performed using a CHI-660D electrochemical workstation (Shanghai Chenhua Co. Ltd., China) with a standard three-electrode cell containing a platinum foil counter electrode, a saturated calomel reference electrode and the working electrode. The working electrodes were fabricated by blending the active material, carbon black and polytetrafluoroethylene (PTFE) at a weight ratio of 8:1:1 and pressed onto Ni foam current collectors (1.0 cm×1.0 cm), and then dried under vacuum at 60°C for 12 h. The measurements were taken in a 6M KOH aqueous electrolyte at room temperature.

3. RESULTS AND DISCUSSION

3.1. XRD analyses and TGA

X-ray diffraction (XRD) was conducted to investigate the crystal structures of RGO/PANI/Co₃O₄ hybrid. Figure.1 presents the XRD pattern of GO, GO/PANI, RGO/PANI and RGO/PANI/Co₃O₄. The GO shows a strong diffraction peak at 11.7° corresponding to the (001) reflection. The XRD survey of RGO/PANI composite shows a wide diffraction peak (15~30°) and three weak diffraction peaks. The peaks at 2θ of 14.6° and 25.1° were attributed to the regularly perpendicular and parallel to the PANI chain, respectively [23]. For RGO/PANI/Co₃O₄, the peak at the 2θ values of 19.1°, 31.4°, 36.8°, 38.7°, 44.9°, 55.7°, 59.5° and 65.3° can be indexed to the (111), (220), (311), (222), (400), (422), (511) and (440) crystal planes of Co₃O₄, respectively (JCPDS card no.43-

1003) [24]. RGO/PANI had similar peaks as GO/PANI, except the evident rise in peak intensity at 26° owing to the incorporative influence of RGO nanosheets [25].

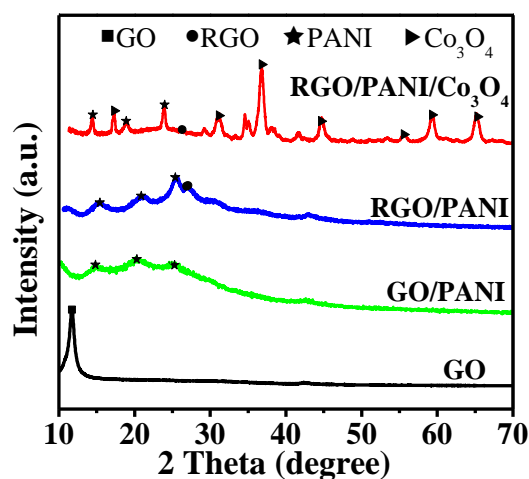


Figure 1. XRD patterns of GO, GO/PANI, RGO/PANI, and RGO/PANI/Co₃O₄.

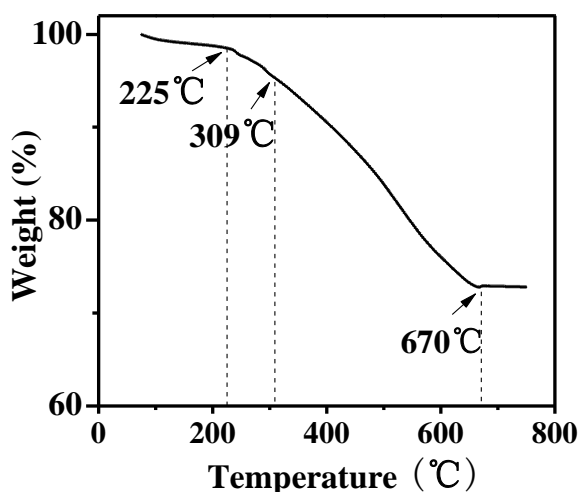


Figure 2. TG curve of as-prepared RGO/PANI/Co₃O₄.

The chemical composition of the obtained sample was illustrated by thermogravimetric analysis (TGA) (Fig. 2). The slight loss of weight displayed by the TG curve at about 225°C was due to the elimination of the physically adsorbed H_2O in composite. The weight started to lose mainly at about 309°C could be ascribed to the calcination of PANI and graphene. PANI and graphene were absolutely removed with the steady of weight after 670°C , which indicated the weight content of Co_3O_4 in RGO/PANI/Co₃O₄ was 72.8%.

3.2. Morphology

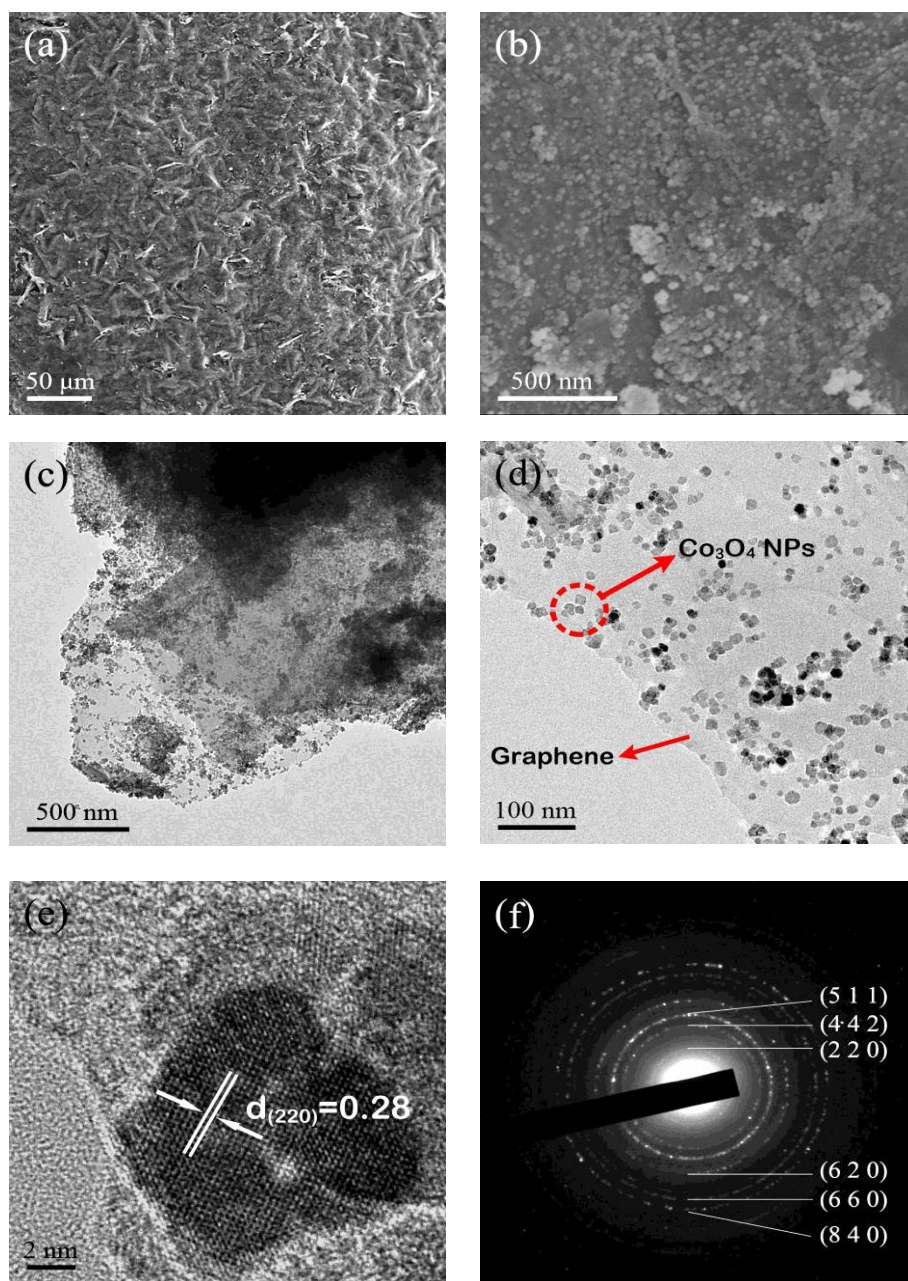


Figure 3. FESEM image (a,b), TEM images (c,d), HRTEM image (e), and corresponding SAED pattern of the as-prepared RGO/PANI/Co₃O₄ composite (f).

The morphology and structures of RGO/PANI/Co₃O₄ was investigated by FESEM and TEM at different magnifications (Fig. 3), respectively. As shown in Fig. 3, the hybrid presents interconnected frameworks of GO. The existence of PANI in the RGO/PANI/Co₃O₄ could be clearly seen in Fig. 3a, and a high-resolution SEM image (Fig. 3b) shows that Co₃O₄ nanoparticles (Co₃O₄ NPs) with a size of ~15 nm were successfully doped homogenously over the GO nanosheets in the process of hydrothermal treatment, which was further revealed by TEM spectra (Fig. 3c, d). Meanwhile, PANI covered the external surface of the GO nanosheets were also found in Fig 3c.

The crystal structure of the RGO/PANI/Co₃O₄ nanocomposite material was further examined by HRTEM analysis (Fig. 3e). Crystal fringes were clearly displayed and the d-spacing of this Co₃O₄ nanoparticle was calculated to be 0.28 nm, corresponding to the (220) plane of Co₃O₄. The SAED pattern within this examined area (Fig. 3f) shows well-defined rings, indicating that the as-prepared Co₃O₄ nanoparticles were polycrystalline. The diffraction rings from inside to outside were indexed to (220), (442), (511), (620), (660) and (840) planes of Co₃O₄ nanoparticles, respectively.

3.3. Raman spectra

Raman spectra was used to further characterize the structures of RGO/PANI/Co₃O₄ hybrid. As showed in Fig. 4, the two broad peaks at 1345 cm⁻¹ (D band) and 1597 cm⁻¹ (G band) indicated the vibration of sp³ C atom and the E_{2g} phonon of sp² C atom of graphene [26]. Fig. 4 also presented the characteristic Raman bands of PANI at 418, 778, 1209, 1332, 1469 cm⁻¹, which could be attributed to out-of-plane C-H wag, imine deformation, C-H vibration in the quinoid/phenyl groups, C-N^{*+} stretching of the bipolaron structure, and the semiquinone radical cation structure in molecular PANI, respectively [27, 28]. Additionally, the peaks centered at about 465, 515, 598, and 674 cm⁻¹ should be related to E_g, E_{2g}¹, F_{2g}², and A_{1g} typical vibration modes of Co₃O₄ [29].

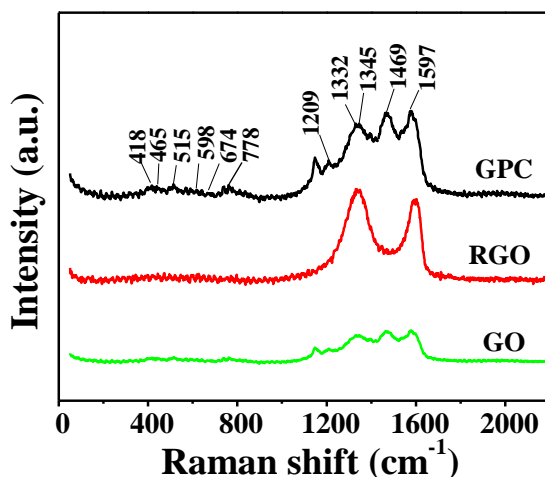


Figure 4. Raman spectra of GO, RGO, and RGO/PANI/Co₃O₄ (GPC).

3.4. XPS

The surface chemical status and the compositions of RGO/PANI/Co₃O₄ were further verified by XPS performed in Fig. 5. The XPS pattern demonstrated that the composite consisted of four elements, C, Co, N, O. Five types of carbon bonds could be clearly observed in the C1s peaks: C-C/C=C (284.5 eV), C-N (285.6 eV), C-O (286.5 eV), C=O (288.2 eV) and O-C=O (290.4 eV) (Fig. 5b). The binding energies located at 779.8 and 796 eV displayed by the high-resolution Co2p spectrum (Fig. 5c) corresponded to Co2p_{3/2} and Co2p_{1/2}, respectively. While the weak peak shakeup satellite at

around 786 eV from the main spin-orbit component was attributed to the interaction between Co and hydroxyl species, which were accorded with the report for Co_3O_4 [20].

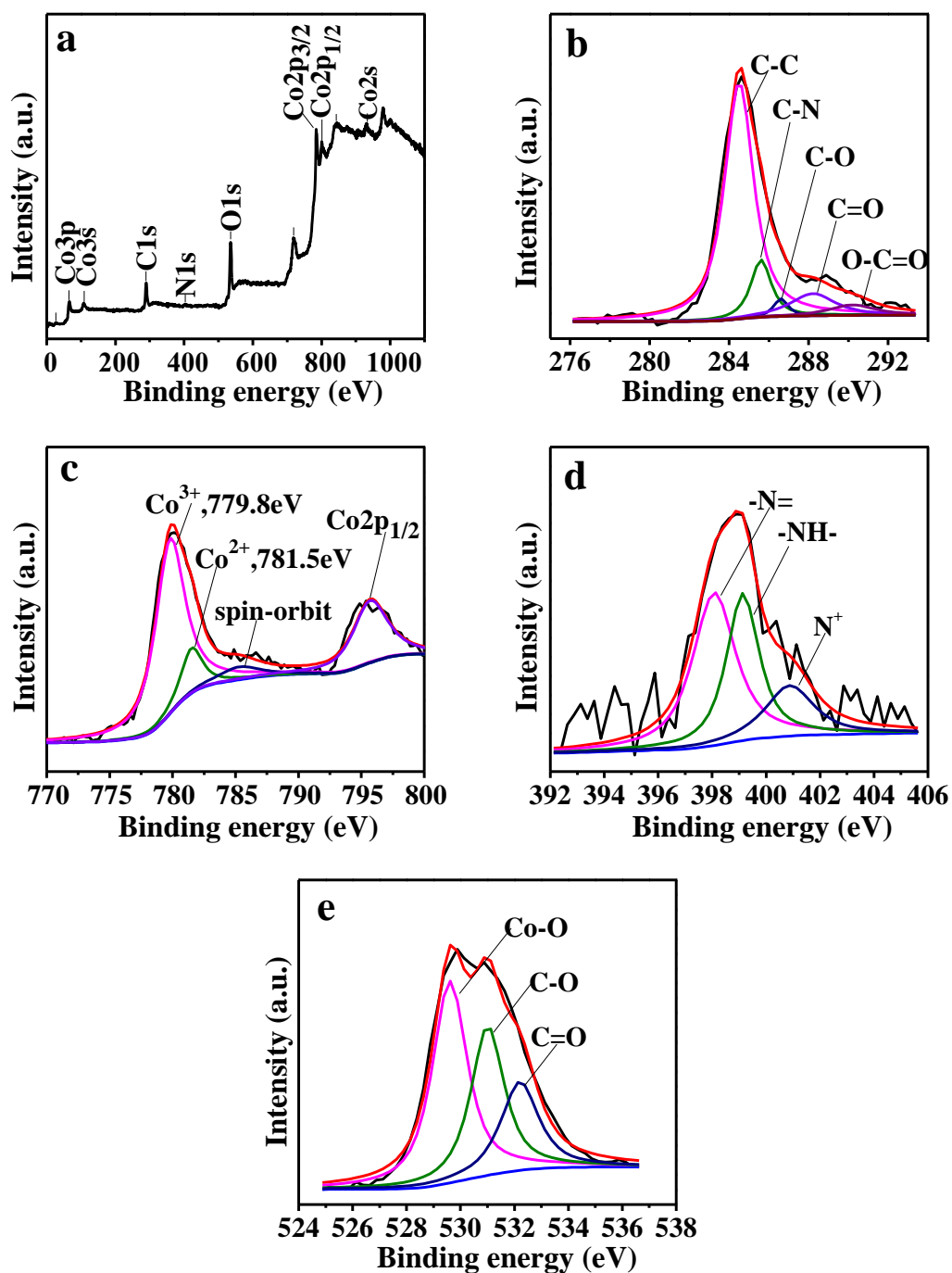


Figure 5. (a) Wide scan survey spectra of RGO/PANI/ Co_3O_4 . (b) XPS C 1s spectra of RGO/PANI/ Co_3O_4 . (c) Co 2p spectra of RGO/PANI/ Co_3O_4 . (d) XPS N 1s spectra of RGO/PANI/ Co_3O_4 . (e) XPS O 1s spectra of RGO/PANI/ Co_3O_4 .

Three Gaussian peaks centered at 398.1, 399.1 and 400.9 eV, which were allocated to benzenoid amine (=N-), quinoid amine (-NH-) and nitrogen cationic radical (N^+), respectively, were carried out by deconvolution of the N 1s core-level XPS of sample (Fig. 5d) [30, 31]. Meanwhile, the

peak located at 529.6 eV in the O 1s XPS spectrum (Fig. 5e) was correspond to O^{2-} , which indicated the existence of Co-O bond in Co_3O_4 .

3.5. Electrochemical properties

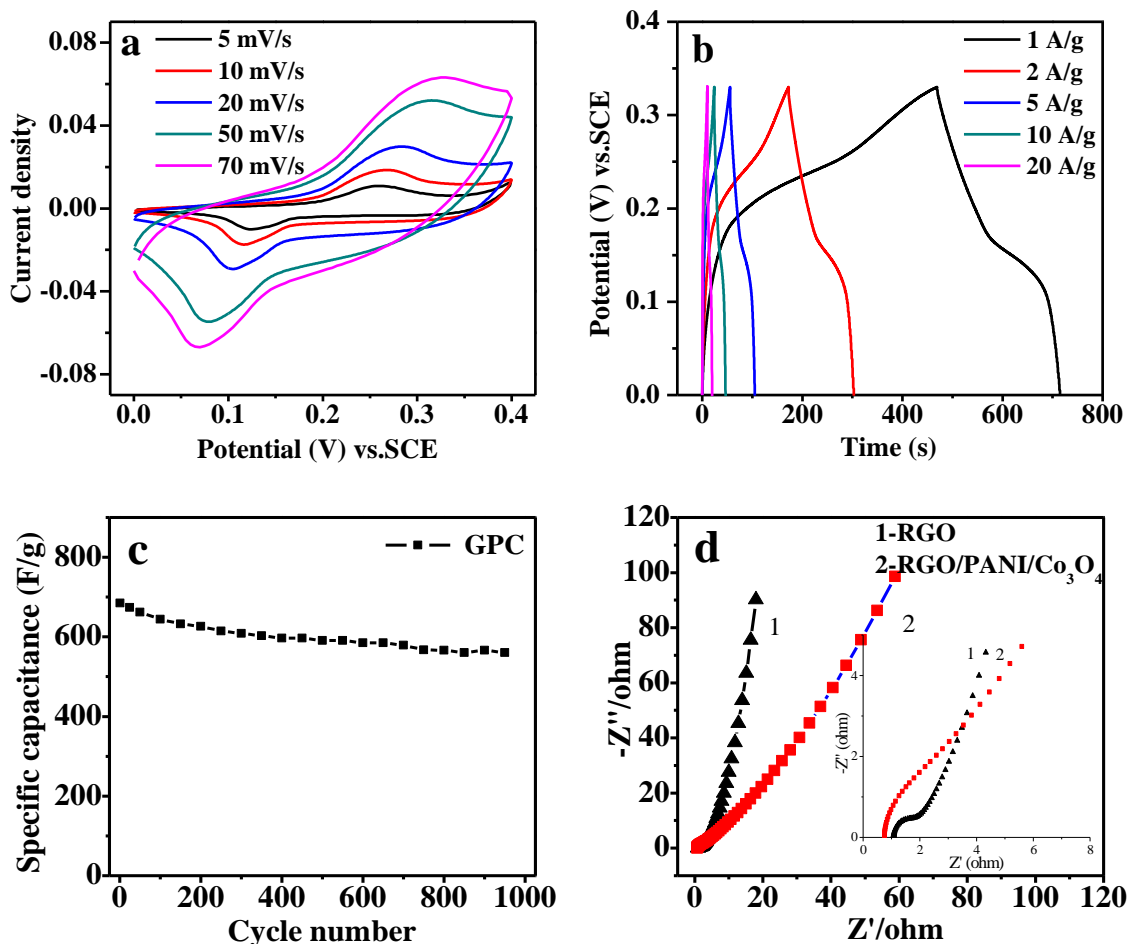


Figure 6. Electrochemical characterizations of RGO/PANI/Co₃O₄: (a) CV curves for RGO/PANI/Co₃O₄ at the scan rate range of 5-70 mV/s in 6 M KOH. (b) Galvanostatic charge/discharge curves of RGO/PANI/Co₃O₄ at different current densities. (c) Cycling performance of RGO/PANI/Co₃O₄ at a current density of 10 A g⁻¹. (d) Nyquist plots of RGO and RGO/PANI/Co₃O₄ electrodes.

The electrochemical performance of RGO/PANI/Co₃O₄ as an active electrode material in a three-electrode system was evaluated by Cyclic voltammetry (CV), galvanostatic charge/discharge experiments, and electrochemical impedance spectroscopy (EIS).

The CV curves of RGO/PANI/Co₃O₄ electrode with various scan rates were shown in Figure. 6a with a voltage range from 0 to 0.4 V in 6 M KOH electrolyte. The reduction peaks and the oxidation peaks varied towards negatively and positively with the increasing of scan rate from 5 to 70 mV s⁻¹, which indicated that the redox reactivities occurred at the interface of electrode/electrolyte.

Additionally, the composite electrode showed outstanding rate performance with the weak shift of redox peaks.

The charge-discharge curves of the RGO/PANI/Co₃O₄ composite electrodes under galvanostatic conditions at varying current densities were depicted in Figure. 6b. The nearly symmetry showed by the curves implied the effect of EDLCs and pseudocapacitive. The specific capacitance could be calculated by following equation: $C = I\Delta t/m\Delta V$, where I represents the discharge current, Δt is the time of a full discharge, m designates the mass of the active materials, and ΔV is voltage change of a full discharge. The specific capacitances of RGO/PANI/Co₃O₄ electrode were calculated to be approximately 789.7, 750, 745.5, 684.9, and 581.8 F g⁻¹ at current densities of 1, 2, 5, 10, and 20 A g⁻¹, respectively, which is superior to other ternary graphene/polyaniline/transition metal oxide reported in the literature (Table 1).

Table 1. Comparison of the specific capacitance of the ternary graphene/polyaniline/transition metal oxide in present work and other reported work in the literature.

Sample	Specific capacitance	Reference
Graphene oxide/polyaniline/MnO ₂ (GO/PANI/MnO ₂)	512 F g ⁻¹ at 0.25 A g ⁻¹	[16]
Graphene/polyaniline/MnO ₂ (RGO/PANI/MnO ₂)	395 F g ⁻¹ at 10 mA cm ⁻²	[17]
Graphene oxide/polyaniline/Co ₃ O ₄ (GO/PANI/Co ₃ O ₄)	713 F g ⁻¹ at 10 mV s ⁻¹	[12]
Graphene/polyaniline (G/PANI)	126 F g ⁻¹ at 10 mV s ⁻¹	[12]
Graphene/polyaniline/Co ₃ O ₄ (RGO/PANI/Co ₃ O ₄)	789.7 F g ⁻¹ at 1 A g ⁻¹	This work

The superior performance of RGO/PANI/Co₃O₄ can be ascribe to the contributions of specific surface area, size of nanoparticles, and Co₃O₄ content. Moreover, it could be ascribe to the prominent capacitance of Co₃O₄ and PANI with pseudocapacitive as well as the intensive interaction between the graphene sheets and evenly distributed Co₃O₄ nanoparticles. And the graphene sheets provided not only the conductivity of the electrode material, but also the rate of charge transfer owing to improvement of the interface between PANI/Co₃O₄ and graphene during hydrothermal treatment. The cycling stability of RGO/PANI/Co₃O₄ composite was also evaluated by galvanostatic charge/discharge measurement at 10 A g⁻¹ in 6 M KOH electrolyte. The capacitance retained 81.8% at 10 A/g during 1000 cycles (Fig. 6c), indicating the high cycling stability of composite.

The properties of RGO/PANI/Co₃O₄ electrode were also evaluated by EIS in the electrolyte interface. The electrochemical impedance spectrum of RGO/PANI/Co₃O₄ electrode after 1000 cycles at 10 A g⁻¹ was measured in the frequency range between 0.01 and 100,000 Hz (Fig. 6d). The Nyquist curves of impedance exhibited a semicircle at high frequency and a relatively linear response at low frequency. The intercepts of the RGO/PANI/Co₃O₄ curve on the real impedance axis, which representing resistance of electrolyte, the intrinsic resistances of the electroactive material and the contact resistance at the interface of the electrode/electrolyte [32, 33], was about 1.1 Ω, lower than values of graphene/activated carbon (~9 Ω) [34], PANI (~6.2 Ω) and RGO/PANI (~10 Ω) [35], because the composite electrode contained graphene with excellent electron conductivity. At the high frequency region, the radius of semicircle displayed the charge-transfer resistance (R_{ct}) at the working

electrode/electrolyte interface [29]. The R_{ct} of RGO/PANI/Co₃O₄ was calculated to be 1.4 Ω through the diameter of the semicircle in the impedance spectrum. Therefore, the electric activity of the material and the electrical conductivity of the entire electrode during the charge-discharge process were promoted with the unique 2D architecture of RGO/PANI/Co₃O₄.

4. CONCLUSION

In a word, a novel ternary composite has been efficiently synthesized through hydrothermal treatment by associating the GO/PANI with Co₃O₄. The RGO/PANI/Co₃O₄ composite possessing interleaved structure exhibited a high specific capacitance of 789.7 F g⁻¹ at a current density of 1 A g⁻¹ and superior cycling stability. The extraordinary electrochemical performance of the RGO/PANI/Co₃O₄ hybrid can be ascribed to the synergistic effects of PANI and Co₃O₄ combined with the effective cross-linker of graphene nanosheets. For supercapacitors, the hybrid is quite a promising and excellent electrode material. Therefore, various multiple composites as electrode materials with wide practical application deserve to be further opened up.

ACKNOWLEDGEMENTS

This research did not receive any specific grant from funding agencies in the public, commercial, or not-for-profit sectors.

References

1. P. J. Hall, M. Mirzaeian, S. I. Fletcher, F. B. Sillars, A. J. R. Rennie, G. O. Shittabey, G. Wilson, A. Cruden, and R. Carter, *Energy & Environmental Science*, 3 (2010) 1238.
2. P. Simon and Y. Gogotsi, *Nature Materials*, 7 (2008) 845.
3. B. G. Choi, M. H. Yang, W. H. Hong, J. W. Choi, and S. H. Yun, *Acs Nano*, 6 (2012) 4020.
4. J. R. Miller and P. Simon, *Science*, 321 (2008) 651.
5. Y. Zhu, S. Murali, M. D. Stoller, A. Velamakanni, R. D. Piner, and R. S. Ruoff, *Carbon*, 48 (2010) 2118.
6. M. Kaempgen, C. K. Chan, J. Ma, Y. Cui, and G. Gruner, *Nano Lett.*, 9 (2009) 1872.
7. T. M. Higgins, D. Mccateer, J. C. M. Coelho, B. M. Sanchez, Z. Gholamvand, G. Moriarty, N. Mcevoy, N. C. Berner, G. S. Duesberg, and V. Nicolosi, *Acs Nano*, 8 (2014) 9567.
8. J. Chen, K. Sheng, P. Luo, C. Li, and G. Shi, *Adv. Mater.*, 24 (2012) 4569.
9. F. Deng, Y. Lin, C. Gao, T. Lin, M. Sun, F. Ye, and Y. Li, *J. Power Sources*, 251 (2014) 202.
10. X. Huang, *Chem. Soc. Rev.*, 41 (2012) 666.
11. S. Stankovich, D. A. Dikin, G. H. B. Dommett, K. M. Kohlhaas, E. J. Zimney, E. A. Stach, R. D. Piner, S. T. Nguyen, and R. S. Ruoff, *Nature*, 442 (2006) 282.
12. K. Zhang, L. L. Zhang, X. S. Zhao, and J. Wu, *Chem. Mater.*, 22 (2010) 1392.
13. P. A. Basnayaka, M. K. Ram, E. K. Stefanakos, and A. Kumar, *Electrochim. Acta*, 92 (2013) 376.
14. Y. Li, Q. Zhang, X. Zhao, P. Yu, L. Wu, and D. Chen, *J. Mater. Chem.*, 22 (2011) 1884.
15. S. Li, D. Wu, C. Cheng, J. Wang, F. Zhang, Y. Su, and X. Feng, *Angew. Chem.*, 52 (2013) 12105.

16. G. Han, Y. Liu, L. Zhang, E. Kan, S. Zhang, J. Tang, and W. Tang, *Scientific Reports*, 4 (2014).
17. B. Mu, W. Zhang, S. Shao, and A. Wang, *PCCP*, 16 (2014) 7872.
18. L. Jing, Z. Y. Yang, Y. F. Zhao, Y. X. Zhang, X. Guo, Y. M. Yan, and K. N. Sun, *J. Mater. Chem.A*, 2 (2014) 1068.
19. H. Zhang, Y. Dai, H. Zhang, W. Wang, Q. Huang, Y. Chen, and L. Pu, *Int. J. Electrochem. Sci.*, 11 (2016) 6279.
20. Q. Guan, J. Cheng, B. Wang, W. Ni, G. Gu, X. Li, L. Huang, G. Yang, and F. Nie, *Acs Applied Materials & Interfaces*, 6 (2014) 7626.
21. X. C. Dong, H. Xu, X. W. Wang, Y. X. Huang, M. B. Chanpark, H. Zhang, L. H. Wang, W. Huang, and P. Chen, *Acs Nano*, 6 (2012) 3206.
22. W. S. Hummers and R. E. Offeman, *J. Am. Chem. Soc.*, 80 (1958) 1339.
23. L. Li, A. R. Raji, H. Fei, Y. Yang, E. L. Samuel, and J. M. Tour, *Acs Applied Materials & Interfaces*, 5 (2013) 6622.
24. S. K. Meher and G. R. Rao, *J. Phys. Chem. C*, 115 (2011) 15646.
25. Y. Li, X. Zhao, P. Yu, and Q. Zhang, *Langmuir*, 29 (2012) 493.
26. C.-Y. Su, Y. Xu, W. Zhang, J. Zhao, X. Tang, C.-H. Tsai, and L.-J. Li, *Chem. Mater.*, 21 (2009) 5674.
27. Q. Zhou, Y. Li, L. Huang, C. Li, and G. Shi, *J. Mater. Chem.A*, 2 (2014) 17489.
28. L. Jing, Z.-Y. Yang, Y.-F. Zhao, Y.-X. Zhang, X. Guo, Y.-M. Yan, and K.-N. Sun, *J. Mater. Chem.A*, 2 (2014) 1068.
29. H. Lin, Q. Huang, J. Wang, J. Jiang, F. Liu, Y. Chen, C. Wang, D. Lu, and S. Han, *Electrochim. Acta*, 191 (2016) 444.
30. O. C. Compton and S. T. Nguyen, *Small*, 6 (2010) 711.
31. R. L. Arechederra, K. Artyushkova, P. Atanassov, and S. D. Minteer, *Acs Applied Materials & Interfaces*, 2 (2010) 3295.
32. F. Luo, J. Li, Y. Lei, W. Yang, H. Yuan, and D. Xiao, *Electrochim. Acta*, 135 (2014) 495.
33. W. Yang, Z. Gao, J. Ma, J. Wang, B. Wang, and L. Liu, *Electrochim. Acta*, 112 (2013) 378.
34. Q. Zhou, J. Gao, C. Li, J. Chen, and G. Shi, *J. Mater. Chem.A*, 1 (2013) 9196.
35. X. Liu, P. Shang, Y. Zhang, X. Wang, Z. Fan, B. Wang, and Y. Zheng, *J. Mater. Chem.A*, 2 (2014) 15273.